



**HAL**  
open science

## Modelling of migration and orientation of endothelial cells on micropatterned polymers

Julie Joie, Y. Lei, Thierry Colin, Marie-Christine Durrieu, Clair Poignard,  
Olivier Saut

► **To cite this version:**

Julie Joie, Y. Lei, Thierry Colin, Marie-Christine Durrieu, Clair Poignard, et al.. Modelling of migration and orientation of endothelial cells on micropatterned polymers. [Research Report] RR-8252, 2013. hal-00795238v1

**HAL Id: hal-00795238**

**<https://inria.hal.science/hal-00795238v1>**

Submitted on 27 Feb 2013 (v1), last revised 14 May 2014 (v2)

**HAL** is a multi-disciplinary open access archive for the deposit and dissemination of scientific research documents, whether they are published or not. The documents may come from teaching and research institutions in France or abroad, or from public or private research centers.

L'archive ouverte pluridisciplinaire **HAL**, est destinée au dépôt et à la diffusion de documents scientifiques de niveau recherche, publiés ou non, émanant des établissements d'enseignement et de recherche français ou étrangers, des laboratoires publics ou privés.



# Modelling of migration and orientation of endothelial cells on micropatterned polymers

J. Joie, Y. Lei, T. Colin, M.-C. Durrieu, C. Pognard, O. Saut

**RESEARCH  
REPORT**

**N° 8252**

February 2013

Project-Teams MC2





## Modelling of migration and orientation of endothelial cells on micropatterned polymers

J. Joie, Y. Lei, T. Colin, M.-C. Durrieu, C. Pognard\*, O. Saut

Project-Teams MC2

Research Report n° 8252 — February 2013 — 17 pages

**Abstract:** Understanding the cell migration on micropatterned polymers, as well as their orientation is a critical issue in tissue engineering, since it is the preliminary step in the blood vessel formation. In this paper, we derive an agent-based model to describe the migration and the orientation of endothelial cells seeded on bioactive micropatterned polymers. The model is obtained thanks to the experimental observations, and it provides numerical results that are quantitatively in accordance with the experimental data.

**Key-words:** Tissue engineering; biomathematical modeling; agent-based model; endothelial cells; migration; differential equations

---

\* Corresponding author: [clair.poignard@inria.fr](mailto:clair.poignard@inria.fr)

**RESEARCH CENTRE  
BORDEAUX – SUD-OUEST**

351, Cours de la Libération  
Bâtiment A 29  
33405 Talence Cedex

## Modélisation de la migration et de l'orientation de cellules endothéliales

**Résumé :** La compréhension de la migration et de l'orientation de cellules contrôlées géométriquement est un point crucial dans le contexte de l'ingénierie tissulaire. Il s'agit en effet de la première étape pour la formation de vaisseaux sanguins. Dans cet article, nous avons établi un modèle d'agent décrivant la migration et l'orientation de cellules endothéliales dispersées sur des plaques composées de polymères bioactifs. Ce modèle est basé sur des considérations expérimentales et nous avons pu obtenir des résultats quantitativement en accord avec ces expériences.

**Mots-clés :** Ingénierie tissulaire ; modélisation bio-mathématique ; modèles d'agents, cellules endothéliales ; migration ; équation différentielles

## Contents

<b>1</b>	<b>Introduction</b>	<b>4</b>
<b>2</b>	<b>Experimental studies</b>	<b>4</b>
<b>3</b>	<b>Description of the model</b>	<b>6</b>
3.1	Net force acting on the cell . . . . .	7
3.1.1	Cell-to-cell attraction force $\mathbf{F}_c$ . . . . .	7
3.1.2	Repulsive force . . . . .	8
3.1.3	Friction force . . . . .	9
3.1.4	Attractive force of the adhesive areas . . . . .	9
3.2	Orientation of the cells . . . . .	10
3.2.1	Heuristics of the alignment . . . . .	10
3.2.2	Differential equation for $\mathbf{L}_i$ . . . . .	10
<b>4</b>	<b>Numerical simulations</b>	<b>11</b>
4.1	Numerical method . . . . .	11
4.2	Fitting the model with the experiments . . . . .	11
4.2.1	Cell shape . . . . .	11
4.2.2	Qualitative results on the cell motility towards the micropatterns . . . . .	12
4.2.3	Quantitative results : alignment of the cells . . . . .	13
<b>5</b>	<b>Conclusion</b>	<b>15</b>

## 1 Introduction

Tissue engineering is the use of combination of cells, engineering, materials, and suitable biochemical factors to improve or replace biological functions [15]. A major problem for the creation of tissue *in vitro* is the lack of functional microvasculature networks. Indeed, the role of capillaries and blood vessels is to supply oxygen and nutrients to the cells, but also to remove waste products and CO<sub>2</sub> [8]. Without an efficient vessel network, the size of cultured tissues is limited by the weak diffusion of nutrients. The understanding of the mechanisms involved in the creation of new blood vessel is therefore crucial.

One strategy to develop clinical implants consists of appropriate utilizations of bioactive materials: bioactive materials may induce *in vivo* regenerative response at the site of damage, whereas when used *in vitro*, they can stimulate the tissue growth for subsequent implantation [1, 12]. Different bioactive ligands have been used to study their effects on cell functions for a better understanding of vascularization [17]. In the aim of promoting angiogenesis in the case of tissue engineering or of inhibiting angiogenesis in the case of cancer, it is important to understand the mechanisms that regulate lumen formation. Successful micropatterning of cells is becoming a key component of this field [7].

Researchers are currently interested in the behavior of cells on substrates that have been patterned by micro- or nano-fabrication [6, 16]. It is known that cell positioning and physiology can be controlled by the substrate on which the cells adhere [2]. Our experiments show that the use of cell adhesion peptides that are micropatterned onto material makes possible the formation of tube-like structures unlike the use of virgin or homogeneously grafted materials [11, 12].

Actually, experimental studies using micropatterned substrates revealed that the cell migration is governed by the geometry of patterns. Endothelial cells so cultured form extensive cell-cell interactions. In some configurations, accumulation of endothelial cell junctions implies that some cells form tube-like structures. The goal of the present paper is to provide a model that describes quantitatively the cell migration towards the micropatterns and the final orientation of the cells on the patches.

In a previous work [3], we have derived a continuous model of cell migration. That approach makes possible the description of the evolution of endothelial cell densities. As described in [3], the results are qualitatively in good agreement with the experiments. In particular we have shown the high influence of the geometry and of the initial density of the cells on the migration. Nevertheless such a continuous model does not take the cell orientation into account, which is an experimental data. Cell orientation on the micropatterns plays a crucial role in the formation of tube-like structure. The aim of this work is to propose a model that can account for cells' orientation. Unlike [3], we do not work with cell density but we consider each cell separately and we describe cell-to-cell interactions for a large number of cells.

The outline of this article is the following: in a first part we present the experimental techniques and the data that are available. We then describe the set of equations defining the model, before presenting numerical results. We also show the consistency of our model, by comparing quantitatively both numerical and experimental data.

## 2 Experimental studies

All the experimental results presented here are taken from [11, 12]. The micropatterned polymers are adhesive areas composed of cell adhesion peptides or growth factors peptides that make the cells adhere. These areas are surrounded by non-adhesive areas on which cells move freely [11]. Human umbilical vein endothelial cells (HUVECs) were isolated from the human umbilical cord vein. HUVECs were isolated and grown on gelatin coated culture flasks in a complete HUVEC

culture medium. HUVECs are seeded onto micropatterned bioactive materials during several hours, then they are washed out. Only the adhered endothelial cells remain on material. The initial density of cells is around 50 000 cells per  $\text{cm}^2$  (see [11]).

We assume (and this is actually confirmed by experiments) that active principles (cell adhesion peptides or growth factors) do not diffuse in the domain. Therefore endothelial cells outside adhesive areas have no mean to "feel" directly these areas. They find out these areas indirectly, by the chemoattractant produced by the cell that are already on the patch. Actually, during the migration phase, we observe that cells have a random motility and stop on adhesive areas. Moreover the attraction of endothelial cells on adhesive areas seems to be higher than the one of cells outside those areas. Note that throughout the paper we do not consider the influence of nutrients and we assume that cells obtain enough nutrients from the material (due to grafted active principles onto material).

In Fig.1, the final position of the cells on two different micropatterns are observed. Fig.1(a) shows the case of thin adhesive areas of 10  $\mu\text{m}$  width and distant from 100  $\mu\text{m}$ , whereas Fig.1(b) shows the end of the migration on large strips (bioactive pattern size: 300  $\mu\text{m}$  and distance between patterns: 100  $\mu\text{m}$ ). For a detailed description of such experiences, one may refer to [11].

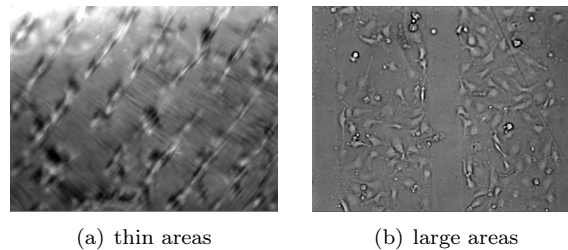


Figure 1: Endothelial cells alignment onto micropatterned polymer (PET) (10 $\mu\text{m}$  (a) and 300  $\mu\text{m}$  (b) stripes of cell adhesion peptides) [11]. The distance between bioactive patterns is 100  $\mu\text{m}$ .

It has been observed that cells tend to gather along the micropatterns. Note that the cells located on the adhesive areas still move along the patch: they are not completely stucked on the adhesive area, but they do not leave the strips. Note also that according to pattern size, endothelial cells line their cytoskeleton to adjust it with the adhesive area.

As presented in [11], the orientation of the endothelial is strongly influenced by the width of the patterns. The figure 2 shows cells on different widths of strips . One can also notice that, with micropatterns of 10  $\mu\text{m}$  thin strips, tubes containing a central lumen may appear [11, 4]. In other words, blood vessels are created from an initial random density of endothelial cells. Such phenomenon is not observed with larger strips [4, 9, 13].

Our goal is to obtain some information on the influence of the micropatterned geometry on both cell migration and alignment. The following facts have been observed experimentally:

- Initially, cells have a random motility and stop on the adhesive areas
- The attractive force between cells is important.
- Cells on adhesive areas more strongly pull their neighbors and still have a very low motility.
- Two cells cannot stack themselves.
- If a part of a cell is located on a strip, it tries to enter totally on the patch.

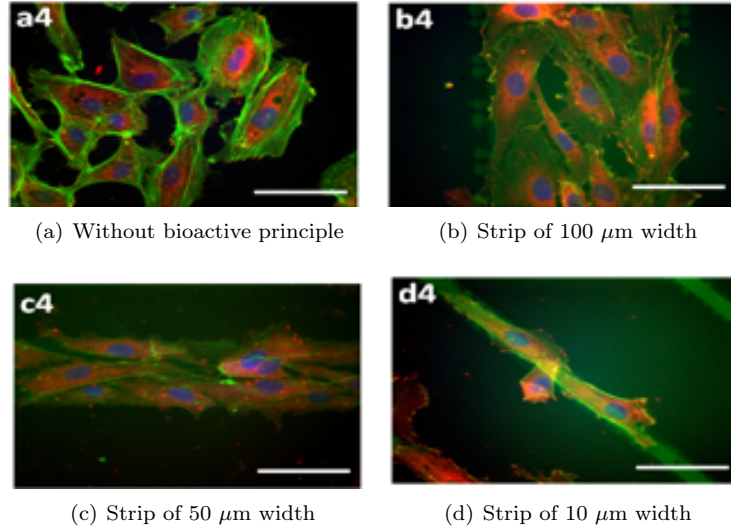


Figure 2: Endothelial cells alignment on different micropatterned polymers (PET) (strips of RGDS peptides), [11]

- Cells line themselves with their neighbors.

We aim at deriving a model that describes precisely these phenomena. Note that since the cell deformation during the migration is a very complex process, which is still poorly understood, we choose to consider simple cell shape, namely in the paper, the cells are ellipses whose parameters depend on the configuration of the experiments.

### 3 Description of the model

Since the experiment data deal with a quite small number of cells, the continuous model derived in [3] cannot provide results that could be quantitatively in accordance with the experiments. The use of a discrete model has been preferred here to describe the cell migration on the micropatterns at the microscopic level. We therefore aim at deriving a model that describes both motility and orientation of a single cell, with respect to its neighbors and its environment.

For the sake of simplicity, we did not consider the cell deformation caused by its motion. In addition, since the cells can be seen as flat<sup>1</sup> and since in most of our data they do not overlap, we consider cells to be bidimensional.

We denote by  $\Omega$  the domain on which cells migrate. This domain is splitted into two parts: the micropatterned domain  $\Omega_\pi$ , on which cells adhere, and the domain  $\Omega \setminus \Omega_\pi$ , on which cells move freely. In the experiments,  $\Omega_\pi$  is mainly composed of disjoint thin strips of polymers, but some experiments have dealt with annulus micropatterns (see Fig. 3(c)). We describe the motion and the orientation of  $N$  cells on the domain  $\Omega$ .

For  $0 \leq i \leq N$ , the  $i^{\text{th}}$  cell at the time  $t$  is characterized by an ellipse centered at the point  $\mathbf{M}_i(t)$  of the surface and whose (major axis) orientation is tracked by the unitary vector  $\mathbf{L}_i(t)$ , as described in Fig. 3(a). The major and minor radii of the ellipse, respectively denoted by  $\Lambda$

<sup>1</sup>According to the experiments, the cells are 25 to 50  $\mu\text{m}$  long, 10 to 20  $\mu\text{m}$  wide and only 1 to 2  $\mu\text{m}$  thick.

and  $\lambda$ , do not depend on time: they are parameters of the model that will be fitted with the experimental data.

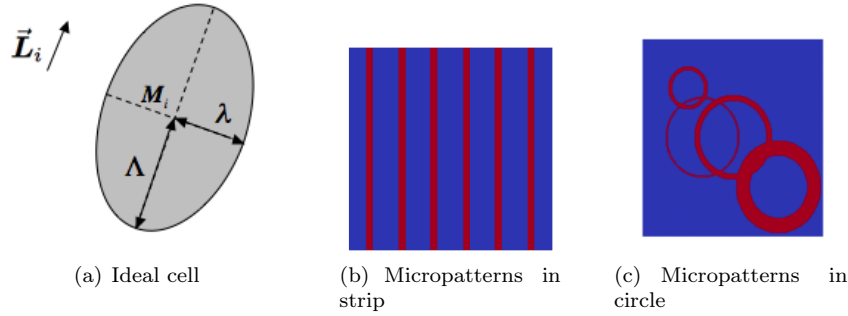


Figure 3: Schematic single cell, and examples of experimental micropatterned domain.

The heuristics of the modeling can be summarized as follows. Using the principle of the second Newton's law, which states that the net force is proportional to the acceleration, we first obtain the motion of  $M_i$ , the center of the ellipsoidal cell. We then obtain the equation on  $L_i$  by analogy with the orientation of a dipole subjected to a field in a bidimensional domain.

### 3.1 Net force acting on the cell

According to the experiments, and to the biological consideration, a single cell is subjected to the four following forces:

- A long range attraction force between the cells  $F_c$ , generated by the chemical signal released by the other cells, so that cells attract themselves.
- A short range repulsion force  $F_r$ , which prevents the overcrowding of the cells.
- A friction force  $F_f$ , which describes the adherence of the domain.
- An attraction force on the patch  $F_a$ , which stacks the cell on the patch thanks to the nutrients.

The differential equation satisfied by the cell center  $M_i$  reads:

$$\ddot{M}_i = F_c - F_r - F_f + F_a. \quad (1)$$

Note that we have normalized cell mass to 1 in Newton's law. This is hidden in the parameters describing each force. Let us write precisely the above forces.

#### 3.1.1 Cell-to-cell attraction force $F_c$

The way that endothelial cells communicate is still not clearly understood, but according to biologists (see [10]), it seems that cells produce chemoattractant that diffuse around them in order to attract their neighbors.

We denote by  $\varphi$  the density of chemoattractant produced by the cells on the domain  $\Omega$ . For each cell, the production of  $\varphi$  is generated by a Gaussian  $\Psi$  supported by the cell, whose

maximum is at the cell center. We assume that the diffusion of  $\varphi$  occurs on a smaller timescale than the cell movement. Therefore  $\varphi$  satisfies the Poisson equation:

$$\Delta\varphi = f_c(\mathbf{x}) \sum_{i=1}^N \Psi(\mathbf{x} - \mathbf{M}_i(t, \mathbf{x})), \quad \forall (t, \mathbf{x}) \in (0, \infty) \times \Omega. \quad (2)$$

Since no chemoattractant is supposed to leave the computational domain, a classical homogeneous Neumann condition is imposed on the boundary of the domain:

$$\partial_{\mathbf{n}}\varphi = 0, \quad \text{on } \partial\Omega, \quad \forall t > 0,$$

where  $\mathbf{n}$  is the normal to  $\partial\Omega$ , outwardly directed from the center to the outer of  $\Omega$ . To close the system, a Gauge condition is necessary. We impose

$$\int_{\partial\Omega} \varphi(t, \mathbf{x}) \, d\mathbf{x} = 0, \quad \forall t > 0. \quad (3)$$

Here above the function  $f_c$  is related to the rate of production of the chemoattractant. We assume that cells produce more chemoattractant on the patch than outside, therefore  $f_c$  is the following piecewise constant function:

$$f_c(\mathbf{x}) = \begin{cases} 1 & \text{if } \mathbf{x} \in \Omega \setminus \Omega_\pi \\ \gamma_c & \text{if } \mathbf{x} \in \Omega_\pi \end{cases}, \quad \text{with } \gamma_c > 1. \quad (4)$$

This corresponds to the fact that cells that are in good condition of adhesion tends to attract the other cells more than the cell whose adhesion is weak.

The attraction force  $\mathbf{F}_c$  is then derived from  $\varphi$ :

$$\mathbf{F}_c(t, \mathbf{x}) = \nabla\varphi(t, \mathbf{x}), \quad \forall (t, \mathbf{x}) \in (0, +\infty) \times \Omega.$$

Note that as the gradient of  $\varphi$  is only involved in  $\mathbf{F}_c$ , the choice of the Gauge condition (3) is not important, since it does not change the gradient of  $\varphi$ .

From the numerical point of view,  $\varphi$  (and thus the attraction force  $\mathbf{F}_c$ ) is computed on the cartesian grid, while the cells move freely in the domain. Therefore, the value of  $\mathbf{F}_c$  is projected on each endothelial cell  $(\mathbf{M}_j)_{j=1}^N$ , using the projection method described by Min and Gibou [14].

### 3.1.2 Repulsive force

It has been experimentally observed that two cells do not overlap. This fact is taken into account by a repulsive term which prevents the cell overcrowding:

$$\mathbf{R}(\mathbf{M}_i) = \sum_{\substack{j=1 \\ j \neq i}}^N \frac{\mathbf{M}_i - \mathbf{M}_j}{\|\mathbf{M}_i - \mathbf{M}_j\|^3}. \quad (5)$$

The power 3 ensures that the repulsive force is an inverse-square law: it is inversely proportional to the square of the distance between 2 cells. Since the cells are ellipsoidal, it is necessary to add a multiplication factor in front of  $\mathbf{R}$ . Actually suppose that two cells are located at the points  $\mathbf{M}_i$  and  $\mathbf{M}_j$  (see Fig 4). When cells are aligned along  $\overline{\mathbf{M}_i\mathbf{M}_j}^\perp$  (see Fig.4(a)), the repulsion force is the lowest since the distance between the cell boundaries is the greatest. On the contrary, in the configuration of Figure 4(b) the cell alignment is parallel to  $\overline{\mathbf{M}_i\mathbf{M}_j}$ , the repulsion force reach

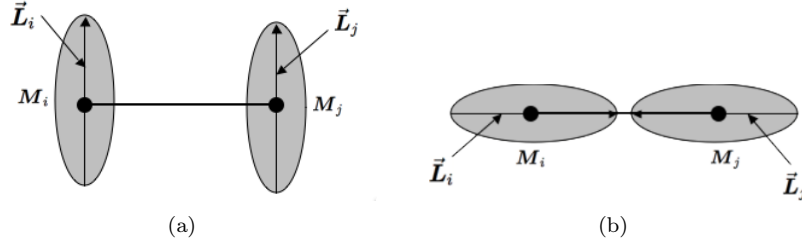


Figure 4: Influence of the cell orientation on the cell-cell distance.

its maximum value. We therefore introduce the factor  $\beta(\mathbf{L}_i)$ , which depends on the orientation of the  $i^{\text{th}}$  cell:

$$\beta(\mathbf{L}_i) = \frac{\Lambda - \lambda}{\lambda} \left( \sum_{\substack{j=1 \\ j \neq i}}^N \left( \left| \frac{\mathbf{M}_i - \mathbf{M}_j}{\|\mathbf{M}_i - \mathbf{M}_j\|} \cdot \mathbf{L}_i \right| + \left| \frac{\mathbf{M}_i - \mathbf{M}_j}{\|\mathbf{M}_i - \mathbf{M}_j\|} \cdot \mathbf{L}_j \right| \right) \right) + 1. \quad (6)$$

The coefficient  $(\Lambda - \lambda)/\lambda$  is introduced in order to take the cell shape into account: for rounded cell it vanishes since there is no cell orientation, and the more elongated the cell, the greater it is. The repulsive force now writes

$$\mathbf{F}_r(\mathbf{L}_i, \mathbf{M}_i) = \gamma_r \beta(\mathbf{L}_i) \mathbf{R}(\mathbf{M}_i), \quad (7)$$

where  $\gamma_r$  is a parameter fitted with the experiments.

### 3.1.3 Friction force

The friction force is proportional to the cell velocity, it thus reads

$$\mathbf{F}_f(\mathbf{M}_i) = \alpha_f f_f(\mathbf{M}_i) \dot{\mathbf{M}}_i,$$

where the friction coefficient  $f_f$  describes the adherence of the domain. Since cells move slowly on the patch,  $f_f(\mathbf{M}_i)$  is a piecewise constant function given by :

$$f_f(\mathbf{M}_i) = \begin{cases} 1 & \text{if } \mathbf{M}_i \in \Omega \setminus \Omega_\pi \\ \gamma_f & \text{if } \mathbf{M}_i \in \Omega_\pi \end{cases}, \quad \text{with } \gamma_f > 1. \quad (8)$$

### 3.1.4 Attractive force of the adhesive areas

If a part of a cell is located on the micropatterned polymer region, it will find nutrients and oxygens on the active principle that will attract the whole cell on the patch. On the contrary, if the cell is completely on the polymer region, or outside this region, the attraction force  $\mathbf{F}_a$  due to the patch vanishes.

We use the above function  $f_f$ , which describes the adherence of the domain, to determine whether the cell is straddling the polymer region and the outer domain. Actually, since the distance between two strips is larger than the cell size, the term

$$f_f(\mathbf{M}_i + \Lambda \mathbf{L}_i) - f_f(\mathbf{M}_i - \Lambda \mathbf{L}_i)$$

vanishes if the point  $\mathbf{M}_i + \Lambda \mathbf{L}_i$  and  $\mathbf{M}_i - \Lambda \mathbf{L}_i$  are on the same domain. It is positive and equal to  $\gamma_f - 1$  if  $\mathbf{M}_i + \Lambda \mathbf{L}_i$  is on the patch and not  $\mathbf{M}_i - \Lambda \mathbf{L}_i$ , and thus the cell will tend to move in the direction of  $\mathbf{L}_i$ . On the other hand, if  $\mathbf{M}_i - \Lambda \mathbf{L}_i$  is on the patch and not  $\mathbf{M}_i + \Lambda \mathbf{L}_i$ , then it equals  $1 - \gamma_f$ , and the cell will tend to move in the direction of  $-\mathbf{L}_i$ . Similar considerations by replacing  $\Lambda$  by  $\lambda$  and  $\mathbf{L}_i$  by  $\mathbf{L}_i^\perp$  ensures that  $\mathbf{F}_a$  is thus given by

$$\begin{aligned} \mathbf{F}_a(\mathbf{M}_i, \mathbf{L}_i) = & \gamma_a (f_f(\mathbf{M}_i + \Lambda \mathbf{L}_i) - f_f(\mathbf{M}_i - \Lambda \mathbf{L}_i)) \mathbf{L}_i \\ & + \gamma_a (f_f(\mathbf{M}_i + \lambda \mathbf{L}_i^\perp) - f_f(\mathbf{M}_i - \lambda \mathbf{L}_i^\perp)) \mathbf{L}_i^\perp, \end{aligned} \quad (9)$$

where  $\gamma_a$  is a numerical parameter.

### 3.2 Orientation of the cells

As mentioned before, the deformation of endothelial cells is a very complex process, which is not taken into account in our simple model. Nevertheless, the cell alignment plays an important role in the tube-like formation. We therefore have chosen to take this alignment behavior into account by modeling the orientation  $\mathbf{L}_i$  of each cell.

#### 3.2.1 Heuristics of the alignment

Before stating the equation satisfied by  $\mathbf{L}_i$ , we introduce the ‘‘alignment’’ vector field  $\Phi$  defined from  $\mathbb{R}^2 \times \mathbb{R}^2$  onto  $\mathbb{R}^2$  by

$$\begin{aligned} \Phi : \quad & \mathbb{R}^2 \times \mathbb{R}^2 \rightarrow \mathbb{R}^2 \\ & (\mathbf{U}, \mathbf{V}) \mapsto (\mathbf{U} \cdot \mathbf{V})(\mathbf{U} \cdot \mathbf{V}^\perp) \mathbf{U}^\perp \end{aligned} \quad (10)$$

In order to understand the above vector field  $\Phi$ , suppose that  $\mathbf{V}$  is a given vector of  $\mathbb{R}^2$ . Let  $\mathbf{U}$  be a time-dependent vector of  $\mathbb{R}^2$  and let  $\theta$  be the angle between  $\mathbf{U}$  and  $\mathbf{V}$  in the left-handed orientation. The orientation of  $\mathbf{U}$  along  $\mathbf{V}$  is easily written by the following ordinary differential equation on  $\theta$ :

$$\dot{\theta} = \sin(2\theta),$$

such that  $\{0, \pi\}$  are stable equilibrium points while  $\{-\pi/2, \pi/2\}$  are unstable. This differential equation can be written in terms of  $\mathbf{U}$  thanks to  $\Phi$ :

$$\dot{\mathbf{U}} = \Phi(\mathbf{U}, \mathbf{V}).$$

#### 3.2.2 Differential equation for $\mathbf{L}_i$

According to the experiments, the cell orientation is driven by three phenomena:

- Alignment along the cell velocity.
- Alignment along the orientation of their neighbors.
- Alignment along the local tangent vector  $\mathbf{S}_i$  of the boundary of micropatterns at the closest point of  $\mathbf{M}_i$ .

We therefore infer the differential equation for  $\mathbf{L}_i$ :

$$\begin{aligned} \dot{\mathbf{L}}_i = & \omega_v \Phi(\mathbf{L}_i, \dot{\mathbf{M}}_i) + \omega_c \sum_{\substack{j=1 \\ j \neq i}}^N \frac{\Phi(\mathbf{L}_i, \mathbf{L}_j)}{\|\mathbf{M}_i - \mathbf{M}_j\|^2} \\ & + \omega_\pi \beta_\pi(\mathbf{M}_i) \Phi(\mathbf{L}_i, \mathbf{S}_i). \end{aligned} \quad (11)$$

Here again it is natural to introduce an inverse-square law for the interaction between two cells. The above function  $\beta_\pi$  is given by

$$\begin{aligned} \beta_\pi(\mathbf{M}_i) = & 4f_f(\mathbf{M}_i) - f_f(\mathbf{M}_i + \Lambda\mathbf{L}_i) - f_f(\mathbf{M}_i - \Lambda\mathbf{L}_i) \\ & - f_f(\mathbf{M}_i + \lambda\mathbf{L}_i) - f_f(\mathbf{M}_i - \lambda\mathbf{L}_i), \end{aligned} \quad (12)$$

it ensures that if the cell is entirely on (or out of) the micropatterns, the cell does not try to align but if the cell is partly on the patch then it tends to align along the direction of the patch. Here above, the parameters  $\omega_v$ ,  $\omega_c$  and  $\omega_\pi$  are homogeneous to the inverse of the characteristic time of each alignment. They will be fitted with the experiments.

## 4 Numerical simulations

### 4.1 Numerical method

The discretization of the time derivatives are made using a "leap-frog" scheme for the acceleration and a centered scheme for the velocity. Initially, cells are randomly distributed on the domain  $\Omega$ .

The Laplace problem (2) is discretized using a centered finite volume scheme (cf [5]). The variables are computed at the center of each element of the mesh. The homogenous Neumann condition is imposed using a penalty method. This allows us to define a general framework to deal with different kinds of geometries (cf Fig. 3(b) and Fig. 3(c)). We use a solver implemented on the academic library `eLYSe`.

### 4.2 Fitting the model with the experiments

In order to study the consistency of our model, we compare the simulation with the experimental results. We focus on experimental results described in [11]. The domain  $\Omega$  is a square of  $1\text{mm}^2$ , on which 500 cells are randomly distributed, in accordance with the experiments. To compute the distribution of the chemoattractant  $\varphi$  given by (2), the domain  $\Omega$  is meshed thanks to a cartesian grid of  $100 \times 100$  elements. Three different widths of the adhesive areas are considered: 10, 50 and 100  $\mu\text{m}$ , with the same spacing of 100  $\mu\text{m}$  between the strips.

#### 4.2.1 Cell shape

In [11], for all three cases, the authors give the cell shapes distribution at the end of the experiments. They measured an approximation of the circularity (cf Fig 5(a)) of the cells corresponding to the rapport of the major axis with the minor axis. They also give the area of the cells on the three different geometries (cf Fig. 5(b)).

These measures determine entirely the cell shape parameter of the model thanks to the relations:

$$\mathcal{C} = \lambda/\Lambda, \quad \mathcal{A} = \pi\Lambda\lambda.$$

Therefore, for each test-case the value of  $\Lambda$  and  $\lambda$  are given by table 1. Since our phenomenological model does not come from physical consideration, the parameters involved in the modeling cannot be measured. Therefore it is essential to fit the parameters with the experiments.

We first consider the experiments with strips of 100  $\mu\text{m}$  width. We then chose the parameters given by table 2 to fit with the experiments. In the next paragraph, the consistency of the model will be shown in the next section by comparing the numerical results with the experiments. We keep the parameters of table 2 and we change the width of the strips as well as the final shape of the cells in accordance with the experiments.

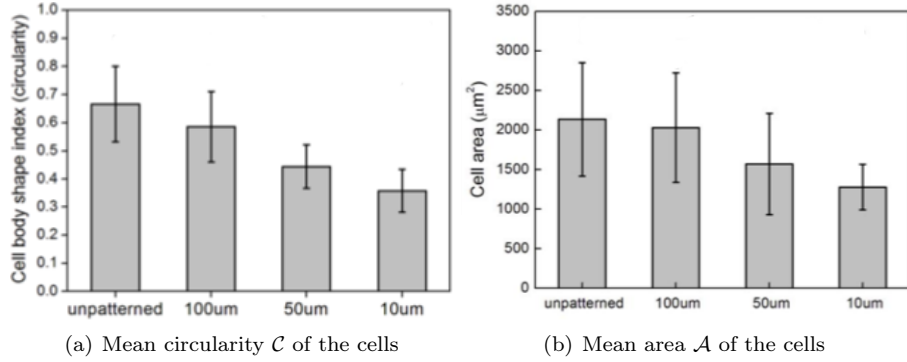
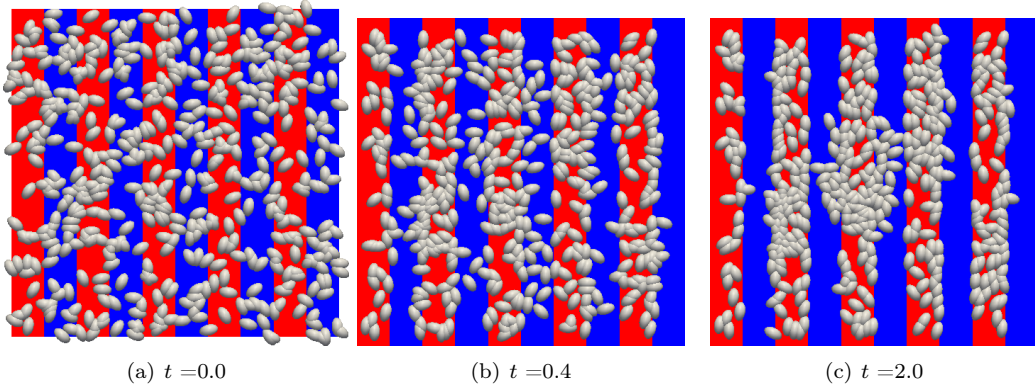


Figure 5: Cells shape informations measured at the end of the experiment. [11]

Strip width	10 $\mu\text{m}$	50 $\mu\text{m}$	100 $\mu\text{m}$
$\Lambda$ : Semi major axis ( $\mu\text{m}$ )	59.6	59.7	59.2
$\lambda$ : Semi minor axis ( $\mu\text{m}$ )	21.4	26.2	34.3

Table 1: Major and minor axes of the cells with respect to the width of the strips.

$\gamma_c$	$\gamma_r$	$\gamma_f$	$\alpha_f$	$\gamma_a$	$\omega_v$	$\omega_c$	$\omega_\pi$
10	$10^{-5}$	120	10	0.05	1	0.005	10

Table 2: Parameters set to fit with the experiments of 100  $\mu\text{m}$ .Figure 6: Position and orientation of endothelial cells on 100  $\mu\text{m}$  strips at different times.

#### 4.2.2 Qualitative results on the cell motility towards the micropatterns

We first provide qualitative results of the cell migration for strips of 100  $\mu\text{m}$  width. In Fig.6, the positions of the endothelial cells at different times are given. The adhesive areas are colored in red, the outer domain in blue and the cells are plotted as white ellipses. In accordance with the experiments, we observe that the cells migrate towards the strips. Note that since some cells remains out of the patches, as for the experiments since the cells do not have enough space on

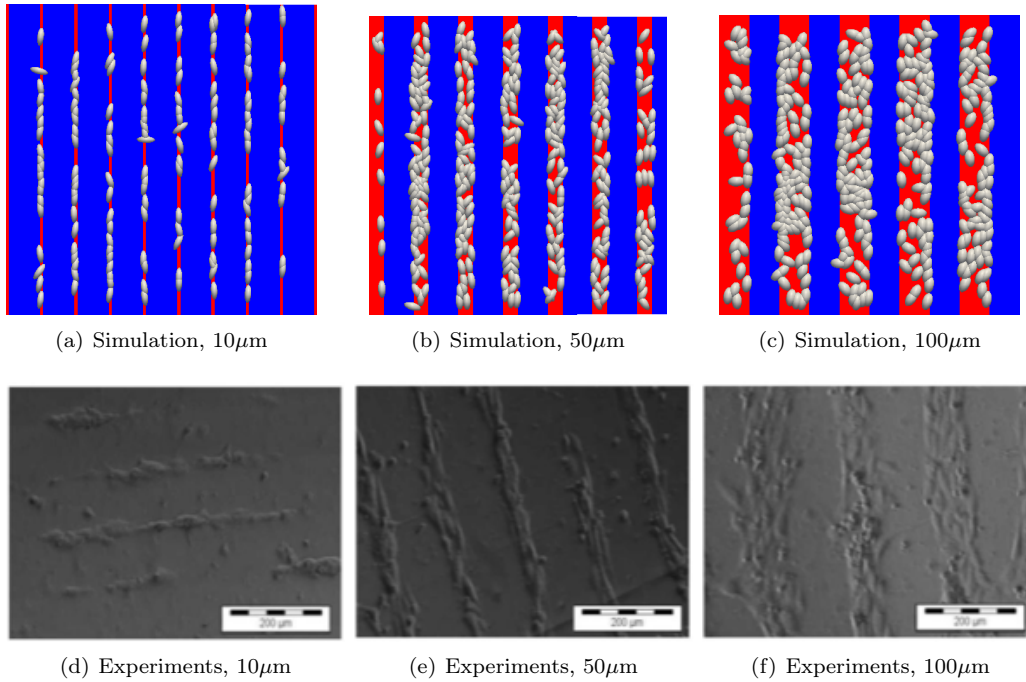


Figure 7: Comparison between experiments [11] and simulations

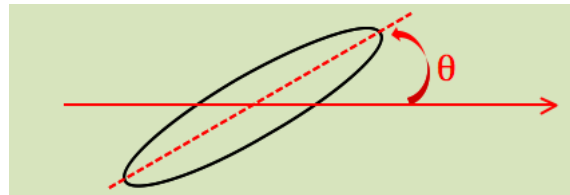


Figure 8: Definition of the angle  $\theta$  for a cell.

the adhesive areas.

In the experiments the cells are washed out before counting. Thus in Fig. 7, we present the final cell position on the patch only, at the end of the simulation (*i.e.* when the cells are almost completely stabilized).

The results are qualitatively in agreement with the experiments.

#### 4.2.3 Quantitative results : alignment of the cells

We now focus on the orientation of the cells in the three previous configurations. In [11], at the end of the experiment, the authors measure the angle  $\theta$  (in degree) between the major axis of a cell with the axis of the adhesive areas as shown in the Fig. 8. For each configuration, six experiences are performed and histograms of the mean values are obtained. This is consistent with the number of experiences performed for each configurations ([10]). When  $\theta$  is less than  $10^\circ$ , we have considered that the cells are aligned with the strip.

We first consider the 100  $\mu\text{m}$  width strips case. We have computed the angle  $\theta$  of the adhered cells for different initial conditions. We present experimental and numerical results in Fig. 9. The results are qualitatively and quantitatively in accordance with the experiments. Experimentally, 27% of the cells are considered to be aligned, numerically, this value is equal to 26.21%. Moreover, the mean value of the cell body alignment angle is equal to 25.9 in [11] and we obtain a very closed value: 25.32. (see also Table 3).

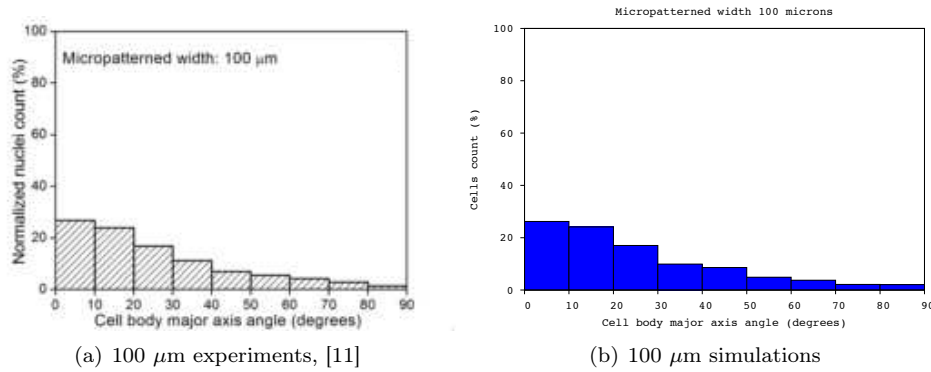


Figure 9: Alignment of the cells on 100 $\mu\text{m}$  strips, comparison between experimental (a) and numerical (b) results.

For the domain composed by 10 $\mu\text{m}$  width strips, the results are also in accordance with the experiments, as shown in Fig. 10.

Note that the number of aligned cells is more important on thin strips. Numerically, 76.12 % of the cells have an angle belonging between  $0^\circ$  and  $10^\circ$  whereas experimentally one obtains 73 % of the cells. The mean alignment angle value obtained numerically is equal to  $8.8^\circ$  and experimentally it is equal to  $8.6^\circ$ .

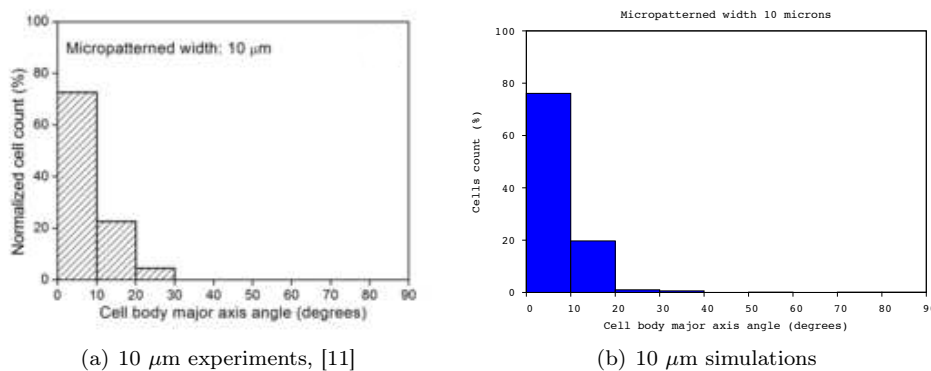


Figure 10: Alignment of the cells on 10  $\mu\text{m}$  strips in the experiments Fig. 10(a) and in the simulation Fig.10(b).

Let us now take 50  $\mu\text{m}$  width strips. As previously, we show, in Fig. 11, the alignment of the cells at the end of the experiment.

The distribution of the angle have qualitatively the expected behavior, the cells are more

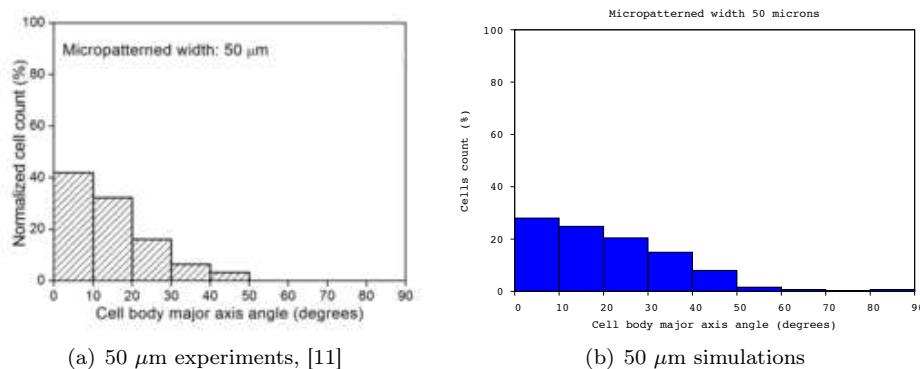


Figure 11: Alignment of the cells on 50 μm strips, comparison between experimental (a) and numerical (b) results.

aligned than in the case of 10 μm strips. Nevertheless, we observe that the values obtained numerically are different from the experiments. One observes that 42 % of the cells are aligned, when we have obtained only 28%. We obtain an angle mean value of 21.1°, which is still in the margin of error of the experimental measurements:  $15.2 \pm 9.6^\circ$ .

## 5 Conclusion

We have provided an agent-based model that describes the cell motility on bioactive micropatterned polymers. The model has been derived by analogy to the Newton laws: the acceleration of the cell is driven by four forces, which describe the cell-cell interactions and the influence of the domain on the cell motility. We also describe the orientation of the cell, similarly to a dipole subjected to a force field. This model involves phenomenological parameters whose values have been estimated to fit the experiments. Changing the configuration of the patches, but keeping the same parameters, we obtain results that are quantitatively in accordance with the experiments. The comparison between the experimental measurement of the cell orientation to the simulation are summarized in table 3. As mentioned above, the numerical results are qualitatively in good agreement with the experimental data.

	% of aligned cells			angle of the mean alignment		
	10 μm	50 μm	100 μm	10 μm	50 μm	100 μm
Exp. Data	73	42	27	$8.6 \pm 6.1^\circ$	$15.2 \pm 9.6^\circ$	$25.9 \pm 15.8^\circ$
Num. Res.	76.12	28	26.21	$8.8^\circ$	$21.1^\circ$	$25.32^\circ$

Table 3: Comparisons of the experiments (Exp. Data.) given by [11] with the numerical simulations (Num. Res.) presented in this paper.

According to these results and to the previous results of [3], we can state that the cell migration as well as the cell alignment with the patches are optimized for a large number of thin strips, rather than for a small number of large strips. Moreover, the forces that we have used are enough to describe both adhesion and orientation of the cells. This may be seen, in some sense, as a basic framework for the description of cell motion on scaffold.

## References

- [1] K. Anselme, P. Davidson, A.M. Popa, M. Liley, and L. Ploux. The interaction of cells and bacteria with surfaces structured at the nanometre scale. *Acta Biomaterialia*, 6:3824–3846, 2010.
- [2] C.S. Chen, M. Mrksich, S. Huang, G.M. Whitesides, and D.E. Ingber. Geometric control of cell life and death. *Science*, 276(5317):1425–1428, 1997.
- [3] T. Colin, M.-C. Durrieu, J. Joie, Y. Lei, Y. Mammeri, C. Poignard, and O. Saut. Modeling of the migration of endothelial cells on bioactive micropatterned polymers. *Mathematical biosciences and engineering*, to appear, 2012.
- [4] L.E. Dike, C.S. Chen, J. Tien, G.M. Whitesides, and D.E. Ingber. Geometric control of switching between growth, apoptosis, and differentiation during angiogenesis using micropatterned substrates. *In Vitro Cell. Dev. Biol.*, 35:441–448, 1999.
- [5] R. Eymard, T. Gallouet, and R. Herbin. *Finite Volume Methods*. Handbook of Numerical Analysis., 2007.
- [6] A. Folch and M. Toner. Microengineering of cellular interactions. *Annu. Rev. Biomed. Eng.*, 2:227–256, 2000.
- [7] Y. Ito. Surface micropatterning to regulate cell functions. *Biomaterials*, 20(23/24):2333–2342, 1999.
- [8] R.K. Jain, P. Au, J. Tam, D.G. Duda, and D. Fukumura. Engineering vascularized tissue. *Nat. Biotechnol.*, 23:821–823, 2005.
- [9] M. Kamei, W.B. Saunders, K.J. Bayless, L. Dye, G.E. Davis, and B.M. Weinstein. Endothelial tubes assemble from intracellular vacuoles in vivo. *Nature*, 442:453–456, 2006.
- [10] Y. Lei. *Biochemical and microscale modification of polymer for endothelial cell angiogenesis*. PhD thesis, Université Bordeaux 1, 2012. [http : //ori - oai.u - bordeaux1.fr/pdf/2012/LEI\\_YIFENG\\_2012.pdf](http://ori-oai.u-bordeaux1.fr/pdf/2012/LEI_YIFENG_2012.pdf).
- [11] Y. Lei, O.F. Zouani, L. Rami, C. Chanseau, and M.-C. Durrieu. Modulation of lumen formation by microgeometrical bioactive cues and migration mode of actin machinery. *Small*, doi:10.1002/sml.201202410, 2012.
- [12] Y. Lei, O.F. Zouani, M. Rémy, C. Ayela, and M.-C. Durrieu. Geometrical microfeature cues for directing tubulogenesis of endothelial cells. *PLoS ONE*, 7(7):e41163, 2012.
- [13] B. Lubarsky and M.A. Krasnow. Tube morphogenesis: making and shaping biological tubes. *Cell*, 112:19–28, 2006.
- [14] C. Min and F. Gibou. A second order accurate level set method on non-graded adaptive cartesian grids. *Journal of Computational Physics*, 225:300–321, 1997.
- [15] R.M. Nerem. Tissue engineering: the hope, the hype, and the future. *Tissue Eng.*, 12(1143-1150), 2006.
- [16] D.V. Nicolau, Taguchi T., H. Taniguchi, H. Tanigawa, and S. Yoshikawa. Patterning neuronal and glia cells on light-assisted functionalized photoresists. *Biosens. Bioelectron.*, 14(3):317–324, 1999.

- [17] E.A. Phelps and A.J. Garcia. Engineering more than a cell: vascularization strategies in tissue engineering. *Curr. Opin. Biotechnol.*, 21:704–709, 2010.



**RESEARCH CENTRE  
BORDEAUX – SUD-OUEST**

351, Cours de la Libération  
Bâtiment A 29  
33405 Talence Cedex

Publisher  
Inria  
Domaine de Voluceau - Rocquencourt  
BP 105 - 78153 Le Chesnay Cedex  
[inria.fr](http://inria.fr)

ISSN 0249-6399